



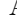






# Measurement of the time-integrated $CP$ asymmetry in $D^0 \rightarrow K_s^0 K_s^0$ decays using opposite-side flavor tagging at Belle and Belle II

I. Adachi<sup>✉</sup>, Y. Ahn<sup>✉</sup>, N. Akopov<sup>✉</sup>, S. Alghamdi<sup>✉</sup>, M. Alhakami<sup>✉</sup>, A. Aloisio<sup>✉</sup>, N. Althubiti<sup>✉</sup>, K. Amos<sup>✉</sup>, M. Angelsmark<sup>✉</sup>, N. Anh Ky<sup>✉</sup>, C. Antonioli<sup>✉</sup>, D. M. Asner<sup>✉</sup>, H. Atmacan<sup>✉</sup>, T. Aushev<sup>✉</sup>, M. Aversano<sup>✉</sup>, R. Ayad<sup>✉</sup>, V. Babu<sup>✉</sup>, H. Bae<sup>✉</sup>, N. K. Baghel<sup>✉</sup>, S. Bahinipati<sup>✉</sup>, P. Bambade<sup>✉</sup>, Sw. Banerjee<sup>✉</sup>, M. Barrett<sup>✉</sup>, M. Bartl<sup>✉</sup>, J. Baudot<sup>✉</sup>, A. Baur<sup>✉</sup>, A. Beaubien<sup>✉</sup>, F. Becherer<sup>✉</sup>, J. Becker<sup>✉</sup>, J. V. Bennett<sup>✉</sup>, F. U. Bernlochner<sup>✉</sup>, V. Bertacchi<sup>✉</sup>, M. Bertemes<sup>✉</sup>, E. Bertholet<sup>✉</sup>, M. Bessner<sup>✉</sup>, S. Bettarini<sup>✉</sup>, B. Bhuyan<sup>✉</sup>, F. Bianchi<sup>✉</sup>, T. Bilka<sup>✉</sup>, D. Biswas<sup>✉</sup>, A. Bobrov<sup>✉</sup>, D. Bodrov<sup>✉</sup>, A. Bondar<sup>✉</sup>, J. Borah<sup>✉</sup>, A. Boschetti<sup>✉</sup>, A. Bozek<sup>✉</sup>, M. Bračko<sup>✉</sup>, P. Branchini<sup>✉</sup>, R. A. Briere<sup>✉</sup>, T. E. Browder<sup>✉</sup>, A. Budano<sup>✉</sup>, S. Bussino<sup>✉</sup>, M. Campajola<sup>✉</sup>, L. Cao<sup>✉</sup>, G. Casarosa<sup>✉</sup>, C. Cecchi<sup>✉</sup>, P. Cheema<sup>✉</sup>, B. G. Cheon<sup>✉</sup>, K. Chilikin<sup>✉</sup>, J. Chin<sup>✉</sup>, K. Chirapatpimol<sup>✉</sup>, H.-E. Cho<sup>✉</sup>, K. Cho<sup>✉</sup>, S.-J. Cho<sup>✉</sup>, S.-K. Choi<sup>✉</sup>, S. Choudhury<sup>✉</sup>, I. Consigny<sup>✉</sup>, L. Corona<sup>✉</sup>, J. X. Cui<sup>✉</sup>, E. De La Cruz-Burelo<sup>✉</sup>, S. A. De La Motte<sup>✉</sup>, G. de Marino<sup>✉</sup>, G. De Pietro<sup>✉</sup>, R. de Sangro<sup>✉</sup>, M. Destefanis<sup>✉</sup>, A. Di Canto<sup>✉</sup>, J. Dingfelder<sup>✉</sup>, Z. Doležal<sup>✉</sup>, I. Domínguez Jiménez<sup>✉</sup>, T. V. Dong<sup>✉</sup>, M. Dorigo<sup>✉</sup>, G. Dujany<sup>✉</sup>, P. Ecker<sup>✉</sup>, D. Epifanov<sup>✉</sup>, R. Farkas<sup>✉</sup>, P. Feichtinger<sup>✉</sup>, T. Ferber<sup>✉</sup>, T. Fillinger<sup>✉</sup>, C. Finck<sup>✉</sup>, G. Finocchiaro<sup>✉</sup>, A. Fodor<sup>✉</sup>, F. Forti<sup>✉</sup>, B. G. Fulsom<sup>✉</sup>, A. Gabrielli<sup>✉</sup>, A. Gale<sup>✉</sup>, E. Ganiev<sup>✉</sup>, M. Garcia-Hernandez<sup>✉</sup>, R. Garg<sup>✉</sup>, G. Gaudino<sup>✉</sup>, V. Gaur<sup>✉</sup>, V. Gautam<sup>✉</sup>, A. Gaz<sup>✉</sup>, A. Gellrich<sup>✉</sup>, D. Ghosh<sup>✉</sup>, H. Ghumaryan<sup>✉</sup>, G. Giakoustidis<sup>✉</sup>, R. Giordano<sup>✉</sup>, A. Giri<sup>✉</sup>, P. Gironella Gironell<sup>✉</sup>, B. Gobbo<sup>✉</sup>, R. Godang<sup>✉</sup>, O. Gogota<sup>✉</sup>, P. Goldenzweig<sup>✉</sup>, W. Gradl<sup>✉</sup>, E. Graziani<sup>✉</sup>, D. Greenwald<sup>✉</sup>, Z. Gruberová<sup>✉</sup>, Y. Guan<sup>✉</sup>, K. Gudkova<sup>✉</sup>, I. Haide<sup>✉</sup>, Y. Han<sup>✉</sup>, H. Hayashii<sup>✉</sup>, S. Hazra<sup>✉</sup>, C. Hearty<sup>✉</sup>, M. T. Hedges<sup>✉</sup>, A. Heidelberg<sup>✉</sup>, G. Heine<sup>✉</sup>, I. Heredia de la Cruz<sup>✉</sup>, M. Hernández Villanueva<sup>✉</sup>, T. Higuchi<sup>✉</sup>, M. Hoek<sup>✉</sup>, M. Hohmann<sup>✉</sup>, P. Horak<sup>✉</sup>, C.-L. Hsu<sup>✉</sup>, T. Humair<sup>✉</sup>, T. Iijima<sup>✉</sup>, K. Inami<sup>✉</sup>, G. Inguglia<sup>✉</sup>, N. Ipsita<sup>✉</sup>, A. Ishikawa<sup>✉</sup>, R. Itoh<sup>✉</sup>, M. Iwasaki<sup>✉</sup>, P. Jackson<sup>✉</sup>, D. Jacobi<sup>✉</sup>, W. W. Jacobs<sup>✉</sup>, D. E. Jaffe<sup>✉</sup>, Q. P. Ji<sup>✉</sup>, S. Jia<sup>✉</sup>, Y. Jin<sup>✉</sup>, A. Johnson<sup>✉</sup>, J. Kandra<sup>✉</sup>, K. H. Kang<sup>✉</sup>, G. Karyan<sup>✉</sup>, T. Kawasaki<sup>✉</sup>, F. Keil<sup>✉</sup>, C. Ketter<sup>✉</sup>, M. Khan<sup>✉</sup>, C. Kiesling<sup>✉</sup>, D. Y. Kim<sup>✉</sup>, J.-Y. Kim<sup>✉</sup>, K.-H. Kim<sup>✉</sup>, K. Kinoshita<sup>✉</sup>, P. Kodyš<sup>✉</sup>, T. Koga<sup>✉</sup>, S. Kohani<sup>✉</sup>, K. Kojima<sup>✉</sup>, A. Korobov<sup>✉</sup>, S. Korpar<sup>✉</sup>, E. Kovalenko<sup>✉</sup>, R. Kowalewski<sup>✉</sup>, P. Križan<sup>✉</sup>, P. Krokovny<sup>✉</sup>, K. Kumara<sup>✉</sup>, T. Kunigo<sup>✉</sup>, A. Kuzmin<sup>✉</sup>, Y.-J. Kwon<sup>✉</sup>, K. Lalwani<sup>✉</sup>, T. Lam<sup>✉</sup>, J. S. Lange<sup>✉</sup>, T. S. Lau<sup>✉</sup>, M. Laurenza<sup>✉</sup>, R. Lebourcher<sup>✉</sup>, F. R. Le Diberder<sup>✉</sup>, M. J. Lee<sup>✉</sup>, C. Lemettais<sup>✉</sup>, P. Leo<sup>✉</sup>, P. M. Lewis<sup>✉</sup>, H.-J. Li<sup>✉</sup>, L. K. Li<sup>✉</sup>, Q. M. Li<sup>✉</sup>, W. Z. Li<sup>✉</sup>, Y. Li<sup>✉</sup>, Y. B. Li<sup>✉</sup>, Y. P. Liao<sup>✉</sup>, J. Libby<sup>✉</sup>, J. Lin<sup>✉</sup>, S. Lin<sup>✉</sup>, V. Lisovskyi<sup>✉</sup>, M. H. Liu<sup>✉</sup>, Q. Y. Liu<sup>✉</sup>, Y. Liu<sup>✉</sup>, Z. Liu<sup>✉</sup>, D. Liventsev<sup>✉</sup>, S. Longo<sup>✉</sup>, C. Lyu<sup>✉</sup>, Y. Ma<sup>✉</sup>, C. Madaan<sup>✉</sup>, M. Maggiora<sup>✉</sup>, S. P. Maharana<sup>✉</sup>, R. Maiti<sup>✉</sup>, G. Mancinelli<sup>✉</sup>, R. Manfredi<sup>✉</sup>, E. Manoni<sup>✉</sup>, M. Mantovano<sup>✉</sup>, D. Marcantonio<sup>✉</sup>, S. Marcello<sup>✉</sup>, C. Marinas<sup>✉</sup>, C. Martellini<sup>✉</sup>, A. Martens<sup>✉</sup>, T. Martinov<sup>✉</sup>, L. Massaccesi<sup>✉</sup>, M. Masuda<sup>✉</sup>, S. K. Maurya<sup>✉</sup>, M. Maushart<sup>✉</sup>, J. A. McKenna<sup>✉</sup>, F. Meier<sup>✉</sup>, M. Merola<sup>✉</sup>, C. Miller<sup>✉</sup>, M. Mirra<sup>✉</sup>, S. Mitra<sup>✉</sup>, K. Miyabayashi<sup>✉</sup>, R. Mizuk<sup>✉</sup>, G. B. Mohanty<sup>✉</sup>, S. Moneta<sup>✉</sup>, H.-G. Moser<sup>✉</sup>, M. Nakao<sup>✉</sup>, H. Nakazawa<sup>✉</sup>, Y. Nakazawa<sup>✉</sup>, M. Naruki<sup>✉</sup>, Z. Natkaniec<sup>✉</sup>, A. Natochii<sup>✉</sup>, M. Nayak<sup>✉</sup>, M. Neu<sup>✉</sup>, S. Nishida<sup>✉</sup>, S. Ogawa<sup>✉</sup>, R. Okubo<sup>✉</sup>, H. Ono<sup>✉</sup>, E. R. Oxford<sup>✉</sup>, G. Pakhlova<sup>✉</sup>, S. Pardi<sup>✉</sup>, K. Parham<sup>✉</sup>, H. Park<sup>✉</sup>, J. Park<sup>✉</sup>, K. Park<sup>✉</sup>, S.-H. Park<sup>✉</sup>, A. Passeri<sup>✉</sup>, S. Patra<sup>✉</sup>, R. Pestotnik<sup>✉</sup>, L. E. Piilonen<sup>✉</sup>, P. L. M. Podesta-Lerma<sup>✉</sup>, T. Podobnik<sup>✉</sup>, A. Prakash<sup>✉</sup>, C. Praz<sup>✉</sup>, S. Prell<sup>✉</sup>, E. Prencipe<sup>✉</sup>, M. T. Prim<sup>✉</sup>, S. Privalov<sup>✉</sup>, H. Purwar<sup>✉</sup>, P. Rados<sup>✉</sup>, G. Raeuber<sup>✉</sup>, S. Raiz<sup>✉</sup>, V. Raj<sup>✉</sup>, K. Ravindran<sup>✉</sup>, J. U. Rehman<sup>✉</sup>, M. Reif<sup>✉</sup>, S. Reiter<sup>✉</sup>, M. Remnev<sup>✉</sup>, L. Reuter<sup>✉</sup>, D. Ricalde Herrmann<sup>✉</sup>, I. Ripp-Baudot<sup>✉</sup>, G. Rizzo<sup>✉</sup>, J. M. Roney<sup>✉</sup>, A. Rostomyan<sup>✉</sup>, N. Rout<sup>✉</sup>, L. Salutari<sup>✉</sup>, D. A. Sanders<sup>✉</sup>, S. Sandilya<sup>✉</sup>, L. Santelj<sup>✉</sup>, V. Savinov<sup>✉</sup>, B. Scavino<sup>✉</sup>, C. Schmitt<sup>✉</sup>, J. Schmitz<sup>✉</sup>, S. Schneider<sup>✉</sup>, G. Schnell<sup>✉</sup>, M. Schnepf<sup>✉</sup>, C. Schwanda<sup>✉</sup>, A. J. Schwartz<sup>✉</sup>, Y. Seino<sup>✉</sup>, A. Selce<sup>✉</sup>, K. Senyo<sup>✉</sup>, J. Serrano<sup>✉</sup>, M. E. Sevier<sup>✉</sup>, C. Sfienti<sup>✉</sup>, W. Shan<sup>✉</sup>, X. D. Shi<sup>✉</sup>, T. Shillington<sup>✉</sup>, J.-G. Shiu<sup>✉</sup>, D. Shtol<sup>✉</sup>, B. Shwartz<sup>✉</sup>,

A. Sibidanov , F. Simon , J. Skorupa , R. J. Sobie , M. Sobotzik , A. Soffer , A. Sokolov , E. Solovieva , S. Spataro , B. Spruck , M. Starić , P. Stavroulakis , S. Stefkova , L. Stoetzer , R. Stroili , Y. Sue , M. Sumihama , N. Suwonjandee , H. Svidras , M. Takizawa , K. Tanida , F. Tenchini , F. Testa , O. Tittel , R. Tiwary , E. Torassa , K. Trabelsi , F. F. Trantou , I. Tsaklidis , M. Uchida , I. Ueda , T. Uglov , K. Unger , Y. Unno , K. Uno , S. Uno , Y. Ushiroda , R. van Tonder , K. E. Varvell , M. Veronesi , A. Vinokurova , V. S. Vismaya , L. Vitale , R. Volpe , A. Vossen , S. Wallner , M.-Z. Wang , A. Warburton , M. Watanabe , S. Watanuki , C. Wessel , E. Won , B. D. Yabsley , S. Yamada , W. Yan , S. B. Yang , J. Yelton , J. H. Yin , K. Yoshihara , J. Yuan , Y. Yusa , L. Zani , M. Zeyrek , B. Zhang , V. Zhilich , J. S. Zhou , Q. D. Zhou , L. Zhu , and R. Žlebčík 

(The Belle and Belle II Collaborations)

We measure the time-integrated  $CP$  asymmetry in  $D^0 \rightarrow K_s^0 K_s^0$  decays reconstructed in  $e^+e^- \rightarrow c\bar{c}$  events collected by the Belle and Belle II experiments. The corresponding data samples have integrated luminosities of 980 and 428 fb $^{-1}$ , respectively. To infer the flavor of the  $D^0$  meson, we exploit the correlation between the flavor of the reconstructed decay and the electric charges of particles reconstructed in the rest of the  $e^+e^- \rightarrow c\bar{c}$  event. This results in a sample which is independent from any other previously used at Belle or Belle II. The result,  $A_{CP}(D^0 \rightarrow K_s^0 K_s^0) = (1.3 \pm 2.0 \pm 0.2)\%$ , where the first uncertainty is statistical and the second systematic, is consistent with previous determinations and with  $CP$  symmetry.

PACS numbers:

## I. INTRODUCTION

Decays of charm hadrons offer a unique avenue for exploring flavor and charge-parity ( $CP$ ) violation in the sector of up-type quarks, which is complementary to the searches performed with strange and beauty hadrons. The dynamics of charm decays is complicated by the presence of non-perturbative QCD effects that are difficult to calculate, making it a test case for both the electroweak and strong interactions. After being first observed in 2019 [1],  $CP$  violation in charm decays has gained renewed attention. The nature of the observed  $CP$  violation has yet to be fully understood, and could be due to enhanced non-perturbative QCD effects or to physics beyond the standard model [2–13]. Flavor and isospin symmetries can be used to relate measurements from different decay modes, helping to constrain non-perturbative QCD effects and identify possible new physics contributions [5, 14, 15]. Hence, searches in additional channels and improved measurements of  $CP$  asymmetries in already explored decay modes are important.

In this paper, we report a measurement of the time-integrated  $CP$  asymmetry in  $D^0 \rightarrow K_s^0 K_s^0$  decays using a combination of Belle and Belle II data, which have integrated luminosities of 980 and 428 fb $^{-1}$ , respectively [16, 17]. The time-integrated  $CP$  asymmetry is defined as

$$A_{CP}(D^0 \rightarrow K_s^0 K_s^0) = \frac{\Gamma(D^0 \rightarrow K_s^0 K_s^0) - \Gamma(\bar{D}^0 \rightarrow K_s^0 K_s^0)}{\Gamma(D^0 \rightarrow K_s^0 K_s^0) + \Gamma(\bar{D}^0 \rightarrow K_s^0 K_s^0)}, \quad (1)$$

where  $\Gamma$  indicates the decay rate integrated over decay time, which includes effects due to  $D^0$ - $\bar{D}^0$  mixing. Experimental measurements of  $A_{CP}(D^0 \rightarrow K_s^0 K_s^0)$  [18–22] are consistent with  $CP$  symmetry within about 1%, putting

them at the upper limit of that predicted by the standard model and in the range where new-physics contributions might be seen [15, 23, 24].

An important part in the measurement of  $A_{CP}(D^0 \rightarrow K_s^0 K_s^0)$  is the ability to determine the production flavor of the neutral  $D$  meson, which is referred to as “tagging.” All measurements performed so far use neutral  $D$  decays originating from the strong-interaction decay  $D^{*+} \rightarrow D^0 \pi^+$ , where the charge of the accompanying pion can be used for tagging. (Charge-conjugate modes are implied throughout the paper, unless stated otherwise.) In this measurement, instead, we use the charm flavor tagger (CFT) described in Ref. [25]. The CFT identifies the flavor of a reconstructed neutral  $D$  meson by exploiting correlations with the electric charges of particles reconstructed in the rest of the  $e^+e^- \rightarrow c\bar{c}$  event. These include those originating from the decay of the other charm hadron produced in the event, as well as those possibly produced in association with the reconstructed  $D$  meson, such as in  $D^{*+} \rightarrow D^0 \pi^+$  decays. To avoid correlations with the recently published  $D^{*+}$ -tagged measurement of Ref. [22], we use an independent dataset where all the candidates previously used are removed. As a consequence, the CFT in this measurement acts as an “opposite-side” tagger using information from the other charm hadron in the event. The CFT is calibrated on large data samples of  $D^0 \rightarrow K^- \pi^+$  decays, following the procedure described in Ref. [25]. The time-integrated  $CP$  asymmetry is then determined from an unbinned maximum-likelihood fit to the two-dimensional distribution of the  $K_s^0 K_s^0$  mass and the CFT output. To avoid potential bias, an arbitrary and undisclosed offset was added to the measured value of  $A_{CP}(D^0 \rightarrow K_s^0 K_s^0)$  when fitting to the data. The offset remained undisclosed until the entire analysis procedure was completed and the determination of all uncertainties was finalized.

The paper is organized as follows. Section II provides an overview of the Belle and Belle II detectors. Section III details the simulation samples used in the measurement. The reconstruction and selection of the signal  $D^0 \rightarrow K_s^0 K_s^0$  decays is presented in Section IV. Determination of the asymmetry is covered in Section V, followed by a discussion of the systematic uncertainties affecting the measurement in Section VI. The final results, and a combination with the  $D^{*+}$ -tagged measurement of Ref. [22], are presented in Section VII.

## II. BELLE AND BELLE II DETECTORS

The Belle experiment [16, 26] operated at the KEKB asymmetric-energy  $e^+e^-$  collider [27, 28] between 1999 and 2010. The detector consisted of a large-solid-angle spectrometer, which included a double-sided silicon-strip vertex detector, a 50-layer central drift chamber, an array of aerogel threshold Cherenkov counters, a barrel-like arrangement of time-of-flight scintillation counters, and an electromagnetic calorimeter comprised of CsI(Tl) crystals. All subdetectors were located inside a superconducting solenoid coil that provided a 1.5 T magnetic field. An iron flux-return yoke, placed outside the coil, was instrumented with resistive-plate chambers to detect  $K_L^0$  mesons and identify muons. Two inner detector configurations were used: a 2.0 cm radius beam pipe and a three-layer silicon vertex detector; and, from October 2003, a 1.5 cm radius beam pipe, a four-layer silicon vertex detector, and a small-inner-cell drift chamber [29].

The Belle II detector [30, 31] is an upgrade with several new subdetectors designed to handle the significantly larger beam-related backgrounds of the new SuperKEKB  $e^+e^-$  collider [32]. It consists of a silicon vertex detector wrapped around a 1 cm radius beam pipe and comprising two inner layers of pixel detectors and four outer layers of double-sided strip detectors, a 56-layer central drift chamber, a time-of-propagation detector, an aerogel ring-imaging Cherenkov detector, and an electromagnetic calorimeter, all located inside the same solenoid as used for Belle. A flux return outside the solenoid is instrumented with resistive-plate chambers, plastic scintillator modules, and an upgraded read-out system to detect muons and  $K_L^0$  mesons. For the data used in this paper, collected between 2019 and 2022, only part of the second layer of the pixel detector, covering 15% of the azimuthal angle, was installed.

For both experiments, the  $z$  axis of the laboratory frame is defined as the central axis of the solenoid, with its positive direction determined by the direction of the electron beam.

## III. SIMULATION

We use simulated event samples to identify sources of background, optimize selection criteria, and validate

the analysis procedure. We generate  $e^+e^- \rightarrow \Upsilon(nS)$  ( $n = 4, 5$ ) events and simulate particle decays with EVTGEN [33]; we generate continuum  $e^+e^- \rightarrow q\bar{q}$  (where  $q$  is a  $u$ ,  $d$ ,  $c$ , or  $s$  quark) with PYTHIA6 [34] for Belle, and with KKMC [35] and PYTHIA8 [36] for Belle II; we simulate final-state radiation with PHOTOS [37, 38]; we simulate detector response using GEANT3 [39] for Belle and GEANT4 [40] for Belle II. Beam backgrounds are taken into account by overlaying random trigger data.

## IV. RECONSTRUCTION AND EVENT SELECTION

We use the Belle II analysis software framework (basf2) to reconstruct both Belle and Belle II data [41, 42]. The Belle data are converted to the Belle II format for basf2 compatibility using the B2BII framework [43].

Events are selected by a trigger based on either the total energy deposited in the electromagnetic calorimeter or the number of charged-particle tracks reconstructed in the central drift chamber. The efficiency of the trigger is found to be close to 100% for signal decays.

Candidate  $K_s^0 \rightarrow \pi^+\pi^-$  decays are reconstructed from combinations of oppositely charged particles that are constrained to originate from a common vertex. These particles are assumed to be pions and the resulting dipion mass is required to be in the  $[0.45, 0.55] \text{ GeV}/c^2$  range. Pairs of  $K_s^0$  candidates are combined to form candidate  $D^0 \rightarrow K_s^0 K_s^0$  decays. We perform a kinematic fit [44] to the  $D^0$  candidates by constraining their momentum directions to point back to the measured position of the beam interaction point, and constraining the masses of the two  $K_s^0$  candidates to the nominal  $K_s^0$  mass [45]. Only candidates whose kinematic fits converge are retained for further analysis. The mass of the  $D^0$  candidate,  $m(K_s^0 K_s^0)$ , is required to be in the range  $[1.84, 2.00] \text{ GeV}/c^2$  to exclude partially reconstructed  $D_s^+ \rightarrow K_s^0 K_s^0 \pi^+$  decays, which peak at lower mass values. The  $D^0$  momentum in the  $e^+e^-$  center-of-mass system is required to be greater than  $2.2 \text{ GeV}/c$  to suppress candidates in which the  $D^0$  meson arises from the decay of a  $B$  meson, as the CFT is trained and calibrated for  $e^+e^- \rightarrow c\bar{c}$  events. Candidates that are also reconstructed in the  $D^{*+}$ -tagged analysis of Ref. [22] are removed.

To suppress  $D^0 \rightarrow K_s^0 \pi^+ \pi^-$  decays, we use the large distance ( $L$ ) between the  $K_s^0$  and  $D^0$  decay vertices resulting from the long  $K_s^0$  lifetime. We introduce the variable  $S_{\min}(K_s^0) = \log[\min(L_1/\sigma_{L_1}, L_2/\sigma_{L_2})]$ , where  $L_{1(2)}$  and  $\sigma_{L_{1(2)}}$  are the distance and its uncertainty for the first (second)  $K_s^0$  candidate, respectively [22]. Candidates satisfying  $\min(L_1/\sigma_{L_1}, L_2/\sigma_{L_2}) \leq 0$  are removed. We require  $S_{\min}(K_s^0)$  to be larger than 1.75 and 2.05 for the Belle and Belle II samples, respectively.

Combinatorial background from two unrelated  $K_s^0$  candidates is suppressed using the output of a boosted decision tree (BDT) trained to discriminate such back-

ground from signal decays [46, 47]. The BDT is trained using simulated  $D^0 \rightarrow K_s^0 K_s^0$  decays as signal, and data candidates populating the  $m(K_s^0 K_s^0)$  sideband  $[1.90, 2.00] \text{ GeV}/c^2$  as background. The input variables to the BDT are selected to effectively separate the signal from the background, while minimizing any correlations with  $m(K_s^0 K_s^0)$  and  $S_{\min}(K_s^0)$ . The input variables are the logarithm of the minimum of the transverse impact parameters of the four final-state pions, the logarithm of the minimum of the longitudinal impact parameters of the four final-state pions, the maximum of the momenta of the final-state pions of the  $K_s^0$  candidate with lower momentum, the minimum of the momenta of the final-state pions of the  $K_s^0$  candidate with lower momentum, the absolute value of the polar angle difference between the final-state pions of the  $K_s^0$  candidate with lower momentum, the invariant masses of the two  $K_s^0$  candidates, the scalar sum of the momenta of the two  $K_s^0$  candidates, the absolute value of the asymmetry between the momenta of the two  $K_s^0$  candidates, the flight-distance of the  $D^0$  candidate divided by its uncertainty, and the logarithm of the  $\chi^2$  probability of the vertex fit of the  $D^0$  candidate. The BDT output distributions for the training samples of signal and background candidates are shown in Figure 1. Due to the additional pixel detector layers and the improved reconstruction performance, the Belle II sample has a better signal-to-background separation as compared to Belle. We require the BDT output to exceed 0.037 and 0.075 for Belle and Belle II, respectively.

The requirements on  $S_{\min}(K_s^0)$  and on the BDT output are optimized simultaneously by maximizing the quantity  $S/\sqrt{S+B}$ , where  $S$  and  $B$  are simulated signal and background yields in a  $3\sigma$   $m(K_s^0 K_s^0)$  range around the signal peak (*i.e.*, the signal region shown in Figure 3), while keeping the residual  $D^0 \rightarrow K_s^0 \pi^+ \pi^-$  background below 3% of the  $D^0 \rightarrow K_s^0 K_s^0$  yield. The 3% threshold ensures that the measured asymmetry cannot be biased by more than about one tenth of the expected statistical uncertainty, as discussed in Section VI. The optimization is done separately for the Belle and Belle II samples. The optimized requirements have signal efficiencies of 55% in Belle and 58% in Belle II, and background rejections of 87% for Belle and 94% for Belle II.

We use the CFT to predict the flavor  $q$  of the selected candidates ( $q = +1$  for  $D^0$ ,  $q = -1$  for  $\bar{D}^0$ ). The tagger also outputs an associated dilution factor  $r$ , which is related to the per-candidate mistag probability  $\omega$  by  $r = 1 - 2\omega$ . We remove untagged candidates, *i.e.*, candidates for which the CFT does not produce any flavor prediction ( $qr = 0$ ), which amount to 0.2% and 0.6% of the total in Belle and Belle II, respectively. We accept all candidates in events where multiple  $D^0$  candidates are reconstructed, which amount to 1% and 0.3% of the total in Belle and Belle II, respectively.

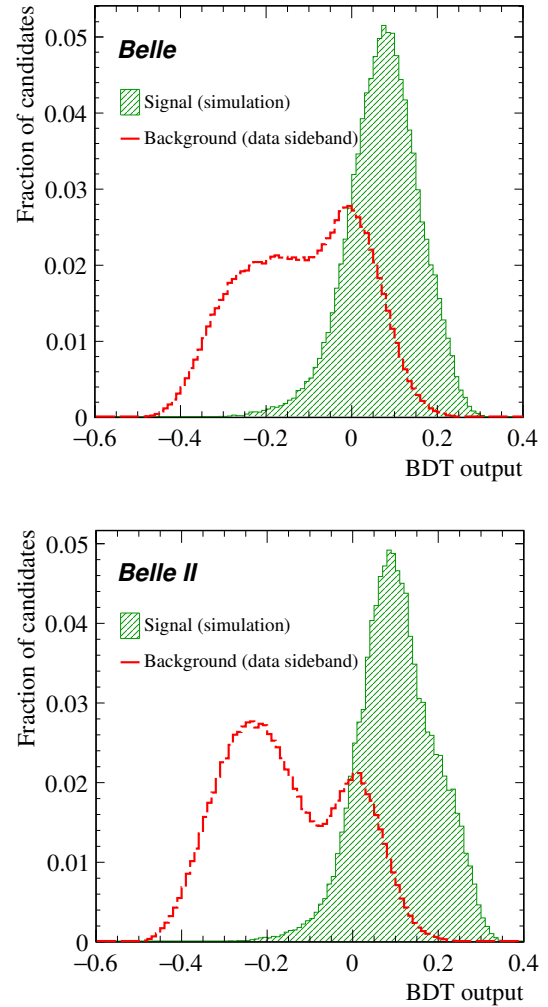


Figure 1: Distributions of the BDT output for the training samples of (green) signal and (red) background candidates in (top) Belle and (bottom) Belle II.

## V. DETERMINATION OF THE $CP$ ASYMMETRY

The  $CP$  asymmetry is determined using an unbinned maximum-likelihood fit to the  $m(K_s^0 K_s^0)$  and  $r$  distributions of the two flavors  $q = \pm 1$ . The  $m(K_s^0 K_s^0)$  distribution discriminates the  $D^0 \rightarrow K_s^0 K_s^0$  signal component from a smooth combinatorial background. The  $qr$  distribution determines the asymmetry between  $D^0$  and  $\bar{D}^0$  candidates. The two-dimensional probability density functions (PDFs) of each component can be factorized into the product of one-dimensional PDFs. The signal  $m(K_s^0 K_s^0)$  PDF,  $P_s(m)$ , is modeled using the sum of two Gaussian distributions. The background PDF,  $P_b(m)$ , is modeled with an exponential distribution. We model the distributions of  $r$ ,  $P_{s,b}(r)$ , using histogram templates extracted directly from the data. For background, we use candidates populating the  $m(K_s^0 K_s^0)$  side-

band  $[1.91, 2.00] \text{ GeV}/c^2$ ; for signal, we subtract the background distribution from that of the candidates in the  $m(K_s^0 K_s^0)$  signal region. Simulation shows that the side-band data describe well the  $r$  distribution of the background candidates in the signal region.

The symbolic expression of the PDF of a single candidate is

$$P(m, q, r | A_{CP}, A_b, \dots) = f_b(1 + qrA_b)P_b(m|\dots)P_b(r) + (1 - f_b)[1 + qd(r|\dots)A_{CP} + q\Delta_d(r|\dots)]P_s(m|\dots)P_s(r), \quad (2)$$

where  $f_b$  is the fraction of background candidates,  $A_b$  is the observed background asymmetry,  $d$  and  $\Delta_d$  are third-order polynomials used to calibrate the per-candidate dilution, and the ellipses (...) indicates other fit parameters omitted here for brevity. All parameters are floated in the fit together with the signal asymmetry  $A_{CP}$ .

The true dilution,  $r^{\text{true}}$ , is expressed as a function of the predicted flavor  $q$  and per-candidate dilution  $r$  using

$$r^{\text{true}}(q, r | p_1, p_2, p_3, \Delta_{p_1}, \Delta_{p_2}, \Delta_{p_3}) = d(r | p_1, p_2, p_3) + q\Delta_d(r | \Delta_{p_1}, \Delta_{p_2}, \Delta_{p_3}), \quad (3)$$

where the coefficients of the polynomials ( $p_1, \dots, \Delta_{p_1}, \dots$ ) are determined by comparing predicted and true dilutions in high-yield data samples of  $D^0 \rightarrow K^- \pi^+$  decays, where the neutral  $D$  flavor is inferred from the charge of the final-state kaon [25] (Figure 2). The tagging power (or effective tagging efficiency), computed from the calibrated per-candidate dilution, is  $(23.52 \pm 0.01)\%$  in Belle and  $(32.71 \pm 0.05)\%$  in Belle II. The tagging power is lower than reported in Ref. [25] due to the removal of the same-side  $D^{*+}$ -tagged candidates. To account for the uncertainties in the calibration parameters, a term constructed from their covariance matrix is included in the likelihood, such that the parameters are Gaussian constrained to their measured values. Thus, the systematic uncertainty associated with the knowledge of the calibration parameters is already taken into account in the statistical uncertainty returned by the fit.

Fits to the simulation and to pseudoexperiments generated by sampling from the PDF show no evidence of a bias in the determinations of the signal yield and asymmetry, nor in their uncertainties.

We perform independent fits to Belle and Belle II data. The fit model describes the data well, as shown in Figure 3. The measured signal yields are  $14490 \pm 340$  in Belle, and  $5180 \pm 120$  in Belle II. The asymmetry is measured to be  $(2.5 \pm 2.7)\%$  in Belle, and  $(-0.1 \pm 3.0)\%$  in Belle II. The uncertainties are statistical only. The two results are in agreement.

## VI. SYSTEMATIC UNCERTAINTIES

We consider the following sources of systematic uncertainties: fit modeling, residual contamination from

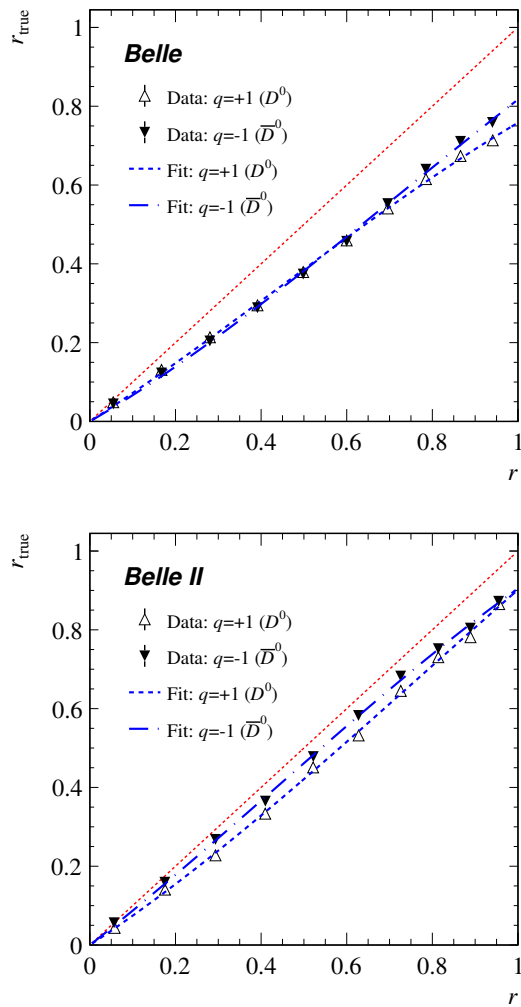


Figure 2: True dilution as a function of the predicted dilution for  $D^0 \rightarrow K^- \pi^+$  and  $\bar{D}^0 \rightarrow K^+ \pi^-$  decays in (top) Belle and (bottom) Belle II data with projections of the calibration fit overlaid. The bisector of the plane (red dotted line) represents the expected relation for perfectly calibrated predicted dilution.

$D^0 \rightarrow K_s^0 \pi^+ \pi^-$  decays, and effects due to the forward-backward asymmetry in  $e^+ e^- \rightarrow c \bar{c}$  production.

We estimate the first using pseudoexperiments generated with the default fit model, and fitted with alternative models derived from data where one of the fit shapes is changed. As alternative models for the mass shapes we use a Johnson  $S_U$  distribution [48] for signal and a second-order polynomial for background. For the  $r$  distributions, we fill alternative histogram templates by varying the definition of the mass sideband. The alternative models give an equally good description of the data as the default models. The observed average differences between measured and generated asymmetries, 0.35% for Belle and 0.10% for Belle II, are assigned as systematic uncertainties.

The residual  $D^0 \rightarrow K_s^0 \pi^+ \pi^-$  background, which is



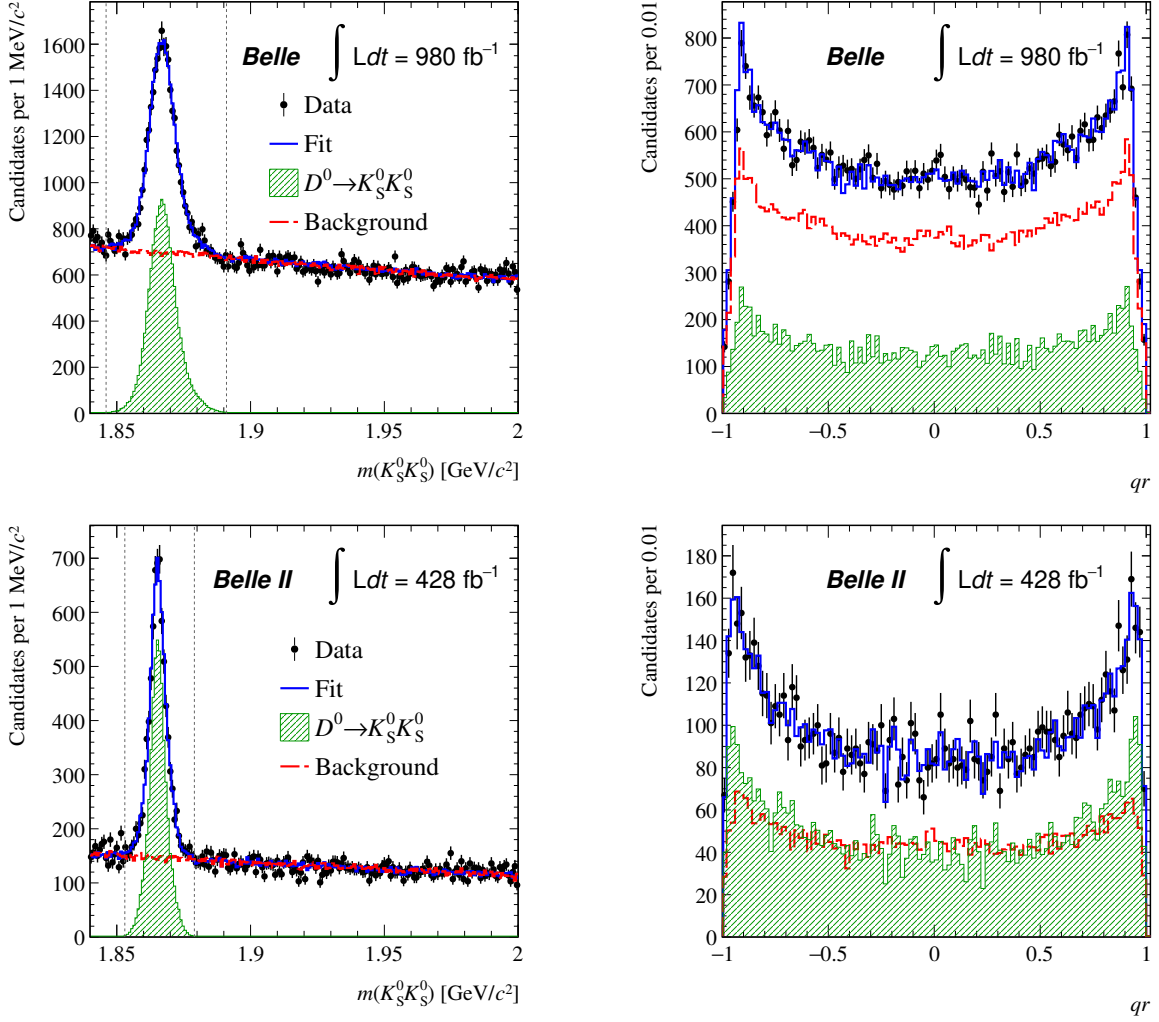


Figure 3: Distributions of (left)  $m(K_S^0 K_S^0)$  and (right)  $qr$  for  $D^0 \rightarrow K_S^0 K_S^0$  candidates in (top) Belle and (bottom) Belle II data, with fit projections overlaid. The  $qr$  distributions are only for candidates in the  $m(K_S^0 K_S^0)$  signal regions indicated by the vertical lines.

indistinguishable from the signal in  $m(K_S^0 K_S^0)$ , is neglected in the fit and counted as part of the signal component. This introduces a bias on the measured asymmetry, which can be estimated as the product of the contamination fraction and the difference between the  $CP$  asymmetries in  $D^0 \rightarrow K_S^0 \pi^+ \pi^-$  and  $D^0 \rightarrow K_S^0 K_S^0$  decays. The contamination fraction is estimated in simulation to be 2.5% for Belle, and 2.3% for Belle II. Given that  $A_{CP}(D^0 \rightarrow K_S^0 \pi^+ \pi^-) - A_{CP}(D^0 \rightarrow K_S^0 K_S^0) < 10\%$  [45], the bias can be conservatively bounded to be smaller than 0.25% for Belle, and 0.23% for Belle II. These values are assigned as systematic uncertainties due to neglecting  $D^0 \rightarrow K_S^0 \pi^+ \pi^-$  contamination.

In  $e^+e^- \rightarrow c\bar{c}$  events, charmed hadrons are produced with a forward-backward asymmetry due to  $\gamma$ - $Z^0$  interference and higher order effects [49–51]. The forward-backward asymmetry is an odd function of the cosine of the polar angle in the center of mass system,  $\cos\theta^*$ .

Since the acceptances of the Belle and Belle II detectors are not the same for  $\cos\theta^* > 0$  and  $\cos\theta^* < 0$ , a charge asymmetry in the production of a given species of charmed hadrons remains. In our measurement, however, we effectively count pairs of charmed hadrons: the signal  $D^0 \rightarrow K_S^0 K_S^0$  and the other (oppositely flavored) charmed hadron of the event, which provides the tagging information. As a result, we expect a negligible effect from the forward-backward asymmetry. To verify this, we weight the reconstructed candidates so that the  $|\cos\theta^*|$  distribution of the signal is the same for candidates with  $\cos\theta^* > 0$  and  $\cos\theta^* < 0$  and redetermine the values of  $A_{CP}$ . As expected, we find variations in  $A_{CP}$  consistent with zero and do not assign any systematic uncertainty due to the forward-backward asymmetry.

Finally, as a cross-check we fit to subsamples of the data defined according to data-taking conditions and find no significant variation of the measured asymmetry.

The total systematic uncertainties, 0.43% for Belle and 0.25% for Belle II, are evaluated as the sums in quadrature of the components due to the fit modeling and the  $D^0 \rightarrow K_s^0 \pi^+ \pi^-$  contamination.

## VII. FINAL RESULTS AND CONCLUSIONS

We measure the time-integrated  $CP$  asymmetry in  $D^0 \rightarrow K_s^0 K_s^0$  decays using a charm-flavor tagging algorithm that exploits the correlation between the flavor of the reconstructed neutral  $D$  meson and the electric charges of particles reconstructed in the rest of the  $e^+e^- \rightarrow c\bar{c}$  event. Using  $980 \text{ fb}^{-1}$  of data collected by Belle and  $428 \text{ fb}^{-1}$  of data collected by Belle II, we obtain

$$A_{CP}(D^0 \rightarrow K_s^0 K_s^0) = (2.5 \pm 2.7 \pm 0.4)\% \quad (4)$$

and

$$A_{CP}(D^0 \rightarrow K_s^0 K_s^0) = (-0.1 \pm 3.0 \pm 0.3)\%, \quad (5)$$

respectively. The first uncertainties are statistical and the second systematic. The two results are in agreement and combined, using the best linear unbiased estimator [52], into

$$A_{CP}(D^0 \rightarrow K_s^0 K_s^0) = (1.3 \pm 2.0 \pm 0.2)\%. \quad (6)$$

In the combination, the systematic uncertainties due to the fit modeling are considered uncorrelated, while those due to the  $D^0 \rightarrow K_s^0 \pi^+ \pi^-$  contamination are considered fully correlated.

The results are also consistent with previous Belle and Belle II determinations based on the independent sample of  $D^{*+}$ -tagged  $D^0 \rightarrow K_s^0 K_s^0$  decays [22]. A combination of the result of this paper with that of Ref. [22],  $(-1.4 \pm 1.3 \pm 0.1)\%$ , yields

$$A_{CP}(D^0 \rightarrow K_s^0 K_s^0) = (-0.6 \pm 1.1 \pm 0.1)\%. \quad (7)$$

This is the most precise determination of  $A_{CP}(D^0 \rightarrow K_s^0 K_s^0)$  to date. It agrees with  $CP$  symmetry and with results from other experiments [18–21].

This work, based on data collected using the Belle II detector, which was built and commissioned prior to March 2019, and data collected using the Belle detector, which was operated until June 2010, was supported by Higher Education and Science Committee of the Republic of Armenia Grant No. 23LCG-1C011; Australian Research Council and Research Grants No. DP200101792, No. DP210101900, No. DP210102831, No. DE220100462, No. LE210100098, and No. LE230100085; Austrian Federal Ministry of Education, Science and Research, Austrian Science Fund (FWF) Grants DOI: 10.55776/P34529, DOI: 10.55776/J4731, DOI: 10.55776/J4625, DOI: 10.55776/M3153, and DOI: 10.55776/PAT1836324, and Horizon 2020 ERC

Starting Grant No. 947006 “InterLeptons”; Natural Sciences and Engineering Research Council of Canada, Compute Canada and CANARIE; National Key R&D Program of China under Contract No. 2024YFA1610503, and No. 2024YFA1610504 National Natural Science Foundation of China and Research Grants No. 11575017, No. 11761141009, No. 11705209, No. 11975076, No. 12135005, No. 12150004, No. 12161141008, No. 12475093, and No. 12175041, and Shandong Provincial Natural Science Foundation Project ZR2022JQ02; the Czech Science Foundation Grant No. 22-18469S and Charles University Grant Agency project No. 246122; European Research Council, Seventh Framework PIEF-GA-2013-622527, Horizon 2020 ERC-Advanced Grants No. 267104 and No. 884719, Horizon 2020 ERC-Consolidator Grant No. 819127, Horizon 2020 Marie Skłodowska-Curie Grant Agreement No. 700525 “NIOBE” and No. 101026516, and Horizon 2020 Marie Skłodowska-Curie RISE project JENNIFER2 Grant Agreement No. 822070 (European grants); L’Institut National de Physique Nucléaire et de Physique des Particules (IN2P3) du CNRS and L’Agence Nationale de la Recherche (ANR) under Grant No. ANR-21-CE31-0009 (France); BMBF, DFG, HGF, MPG, and AvH Foundation (Germany); Department of Atomic Energy under Project Identification No. RTI 4002, Department of Science and Technology, and UPES SEED funding programs No. UPES/R&D-SEED-INFRA/17052023/01 and No. UPES/R&D-SOE/20062022/06 (India); Israel Science Foundation Grant No. 2476/17, U.S.-Israel Binational Science Foundation Grant No. 2016113, and Israel Ministry of Science Grant No. 3-16543; Istituto Nazionale di Fisica Nucleare and the Research Grants BELLE2, and the ICSC – Centro Nazionale di Ricerca in High Performance Computing, Big Data and Quantum Computing, funded by European Union – NextGenerationEU; Japan Society for the Promotion of Science, Grant-in-Aid for Scientific Research Grants No. 16H03968, No. 16H03993, No. 16H06492, No. 16K05323, No. 17H01133, No. 17H05405, No. 18K03621, No. 18H03710, No. 18H05226, No. 19H00682, No. 20H05850, No. 20H05858, No. 22H00144, No. 22K14056, No. 22K21347, No. 23H05433, No. 26220706, and No. 26400255, and the Ministry of Education, Culture, Sports, Science, and Technology (MEXT) of Japan; National Research Foundation (NRF) of Korea Grants No. 2016R1-D1A1B-02012900, No. 2018R1-A6A1A-06024970, No. 2021R1-A6A1A-03043957, No. 2021R1-F1A-1060423, No. 2021R1-F1A-1064008, No. 2022R1-A2C-1003993, No. 2022R1-A2C-1092335, No. RS-2023-00208693, No. RS-2024-00354342 and No. RS-2022-00197659, Radiation Science Research Institute, Foreign Large-Size Research Facility Application Supporting project, the Global Science Experimental Data Hub Center, the Korea Institute of Science and Technology Information (K24L2M1C4) and KREONET/GLORIAD; Universiti Malaya RU

grant, Akademi Sains Malaysia, and Ministry of Education Malaysia; Frontiers of Science Program Contracts No. FOINS-296, No. CB-221329, No. CB-236394, No. CB-254409, and No. CB-180023, and SEP-CINVESTAV Research Grant No. 237 (Mexico); the Polish Ministry of Science and Higher Education and the National Science Center; the Ministry of Science and Higher Education of the Russian Federation and the HSE University Basic Research Program, Moscow; University of Tabuk Research Grants No. S-0256-1438 and No. S-0280-1439 (Saudi Arabia), and Researchers Supporting Project number (RSPD2025R873), King Saud University, Riyadh, Saudi Arabia; Slovenian Research Agency and Research Grants No. J1-50010 and No. P1-0135; Ikerbasque, Basque Foundation for Science, State Agency for Research of the Spanish Ministry of Science and Innovation through Grant No. PID2022-136510NB-C33, Spain, Agencia Estatal de Investigacion, Spain Grant No. RYC2020-029875-I and Generalitat Valenciana, Spain Grant No. CIDEGENT/2018/020; the Swiss National Science Foundation; The Knut and Alice Wallenberg Foundation (Sweden), Contracts No. 2021.0174 and No. 2021.0299; National Science and Technology Council, and Ministry of Education (Taiwan); Thailand Center of Excellence in Physics; TUBITAK ULAKBIM (Turkey); National Research

Foundation of Ukraine, Project No. 2020.02/0257, and Ministry of Education and Science of Ukraine; the U.S. National Science Foundation and Research Grants No. PHY-1913789 and No. PHY-2111604, and the U.S. Department of Energy and Research Awards No. DE-AC06-76RLO1830, No. DE-SC0007983, No. DE-SC0009824, No. DE-SC0009973, No. DE-SC0010007, No. DE-SC0010073, No. DE-SC0010118, No. DE-SC0010504, No. DE-SC0011784, No. DE-SC0012704, No. DE-SC0019230, No. DE-SC0021274, No. DE-SC0021616, No. DE-SC0022350, No. DE-SC0023470; and the Vietnam Academy of Science and Technology (VAST) under Grants No. NVCC.05.12/22-23 and No. DL0000.02/24-25.

These acknowledgements are not to be interpreted as an endorsement of any statement made by any of our institutes, funding agencies, governments, or their representatives.

We thank the SuperKEKB team for delivering high-luminosity collisions; the KEK cryogenics group for the efficient operation of the detector solenoid magnet and IBelle on site; the KEK Computer Research Center for on-site computing support; the NII for SINET6 network support; and the raw-data centers hosted by BNL, DESY, GridKa, IN2P3, INFN, PNNL/EMSL, and the University of Victoria.

- 
- [1] LHCb collaboration, R. Aaij *et al.*, *Observation of CP violation in charm decays*, Phys. Rev. Lett. **122** (2019) 211803, [arXiv:1903.08726](#).
  - [2] M. Chala, A. Lenz, A. V. Rusov, and J. Scholtz,  $\Delta A_{CP}$  within the Standard Model and beyond, JHEP **07** (2019) 161, [arXiv:1903.10490](#).
  - [3] A. Dery and Y. Nir, *Implications of the LHCb discovery of CP violation in charm decays*, JHEP **12** (2019) 104, [arXiv:1909.11242](#).
  - [4] L. Calibbi, T. Li, Y. Li, and B. Zhu, *Simple model for large CP violation in charm decays, B-physics anomalies, muon  $g - 2$  and dark matter*, JHEP **10** (2020) 070, [arXiv:1912.02676](#).
  - [5] Y. Grossman and S. Schacht, *The emergence of the  $\Delta U = 0$  rule in charm physics*, JHEP **07** (2019) 020, [arXiv:1903.10952](#).
  - [6] H.-Y. Cheng and C.-W. Chiang, *Revisiting CP violation in  $D \rightarrow PP$  and  $VP$  decays*, Phys. Rev. D **100** (2019) 093002, [arXiv:1909.03063](#).
  - [7] A. J. Buras, P. Colangelo, F. De Fazio, and F. Lopalco, *The charm of 331*, JHEP **10** (2021) 021, [arXiv:2107.10866](#).
  - [8] S. Schacht and A. Soni, *Enhancement of charm CP violation due to nearby resonances*, Phys. Lett. B **825** (2022) 136855, [arXiv:2110.07619](#).
  - [9] S. Schacht, *A U-spin anomaly in charm CP violation*, JHEP **03** (2023) 205, [arXiv:2207.08539](#).
  - [10] I. Bediaga, T. Frederico, and P. C. Magalhães, *Enhanced Charm CP Asymmetries from Final State Interactions*, Phys. Rev. Lett. **131** (2023) 051802, [arXiv:2203.04056](#).
  - [11] R. Bause *et al.*, *U-spin-CP anomaly in charm*, Phys. Rev. D **108** (2023) 035005, [arXiv:2210.16330](#).
  - [12] A. Pich, E. Solomonidi, and L. Vale Silva, *Final-state interactions in the CP asymmetries of charm-meson two-body decays*, Phys. Rev. D **108** (2023) 036026, [arXiv:2305.11951](#).
  - [13] M. Gavrilova, Y. Grossman, and S. Schacht, *Determination of the  $D \rightarrow \pi\pi$  ratio of penguin over tree diagrams*, Phys. Rev. D **109** (2024) 033011, [arXiv:2312.10140](#).
  - [14] G. Hiller, M. Jung, and S. Schacht, *SU(3)-flavor anatomy of nonleptonic charm decays*, Phys. Rev. D **87** (2013) 014024, [arXiv:1211.3734](#).
  - [15] F. Buccella, A. Paul, and P. Santorelli, *SU(3)<sub>F</sub> breaking through final state interactions and CP asymmetries in  $D \rightarrow PP$  decays*, Phys. Rev. D **99** (2019) 113001, [arXiv:1902.05564](#).
  - [16] Belle collaboration, J. Brodzicka *et al.*, *Physics achievements from the Belle experiment*, PTEP **2012** (2012) 04D001, [arXiv:1212.5342](#).
  - [17] Belle II collaboration, I. Adachi *et al.*, *Measurement of the integrated luminosity of data samples collected during 2019-2022 by the Belle II experiment*, Chin. Phys. C **49** (2025) 013001, [arXiv:2407.00965](#).
  - [18] CLEO collaboration, G. Bonvicini *et al.*, *Search for CP violation in  $D^0 \rightarrow K_S^0 \pi^0$  and  $D^0 \rightarrow \pi^0 \pi^0$  and  $D^0 \rightarrow K_S^0 K_S^0$  decays*, Phys. Rev. D **63** (2001) 071101, [arXiv:hep-ex/0012054](#).
  - [19] LHCb collaboration, R. Aaij *et al.*, *Measurement of the time-integrated CP asymmetry in  $D^0 \rightarrow K_S^0 K_S^0$  decays*, JHEP **10** (2015) 055, [arXiv:1508.06087](#).
  - [20] LHCb collaboration, R. Aaij *et al.*, *Measurement of CP*



- asymmetry in  $D^0 \rightarrow K_S^0 K_S^0$  decays, Phys. Rev. D **104** (2021) L031102, [arXiv:2105.01565](#).
- [21] CMS collaboration, A. Hayrapetyan *et al.*, Search for CP violation in  $D^0 \rightarrow K_S^0 K_S^0$  decays in proton-proton collisions at  $\sqrt{s} = 13$  TeV, [arXiv:2405.11606](#).
- [22] Belle and Belle II collaborations, I. Adachi *et al.*, Measurement of the time-integrated CP asymmetry in  $D^0 \rightarrow K_S^0 K_S^0$  decays using Belle and Belle II data, Phys. Rev. D **111** (2025) 012015, [arXiv:2411.00306](#).
- [23] J. Brod, A. L. Kagan, and J. Zupan, Size of direct CP violation in singly Cabibbo-suppressed D decays, Phys. Rev. D **86** (2012) 014023, [arXiv:1111.5000](#).
- [24] U. Nierste and S. Schacht, CP violation in  $D^0 \rightarrow K_S^0 K_S^0$ , Phys. Rev. D **92** (2015) 054036, [arXiv:1508.00074](#).
- [25] Belle II collaboration, I. Adachi *et al.*, Novel method for the identification of the production flavor of neutral charmed mesons, Phys. Rev. D **107** (2023) 112010, [arXiv:2304.02042](#).
- [26] Belle collaboration, A. Abashian *et al.*, The Belle detector, Nucl. Instrum. Meth. **479** (2002) 117.
- [27] S. Kurokawa *et al.*, Overview of the KEKB accelerators, Nucl. Instrum. Meth. **449** (2003) 1.
- [28] T. Abe *et al.*, Achievements of KEKB, PTEP **2013** (2013) 03A001.
- [29] Z. Natkaniec *et al.*, Status of the Belle silicon vertex detector, Nucl. Instrum. Meth. A **560** (2006) 1.
- [30] Belle II collaboration, T. Abe *et al.*, Belle II Technical Design Report, [arXiv:1011.0352](#).
- [31] W. Altmannshofer *et al.*, The Belle II physics book, PTEP **2019** (2019) 123C01, Erratum *ibid.* **2020** (2020) 029201, [arXiv:1808.10567](#).
- [32] K. Akai, K. Furukawa, and H. Koiso, SuperKEKB collider, Nucl. Instrum. Meth. **A907** (2018) 188, [arXiv:1809.01958](#).
- [33] D. J. Lange, The EvtGen particle decay simulation package, Nucl. Instrum. Meth. **A462** (2001) 152.
- [34] T. Sjöstrand, S. Mrenna, and P. Z. Skands, PYTHIA 6.4 Physics and Manual, JHEP **05** (2006) 026, [arXiv:hep-ph/0603175](#).
- [35] S. Jadach, B. F. L. Ward, and Z. Was, The precision Monte Carlo event generator KK for two-fermion final states in  $e^+e^-$  collisions, Comput. Phys. Commun. **130** (2000) 260, [arXiv:hep-ph/9912214](#).
- [36] T. Sjöstrand *et al.*, An Introduction to PYTHIA 8.2, Comput. Phys. Commun. **191** (2015) 159, [arXiv:1410.3012](#).
- [37] E. Barberio, B. van Eijk, and Z. Was, PHOTOS: A universal Monte Carlo for QED radiative corrections in decays, Comput. Phys. Commun. **66** (1991) 115.
- [38] E. Barberio and Z. Was, PHOTOS: A Universal Monte Carlo for QED radiative corrections. Version 2.0, Comput. Phys. Commun. **79** (1994) 291.
- [39] R. Brun *et al.*, GEANT: detector description and simulation tool; March 1994, CERN Program Library, CERN, Geneva, 1993. Long Writeup W5013.
- [40] GEANT4 collaboration, S. Agostinelli *et al.*, GEANT4: A simulation toolkit, Nucl. Instrum. Meth. **A506** (2003) 250.
- [41] Belle II Framework Software Group, T. Kuhr *et al.*, The Belle II Core Software, Comput. Softw. Big Sci. **3** (2019) 1, [arXiv:1809.04299](#).
- [42] Belle II collaboration, Belle II Analysis Software Framework (basf2), <https://doi.org/10.5281/zenodo.5574115>.
- [43] M. Gelb *et al.*, B2BII: Data Conversion from Belle to Belle II, Comput. Softw. Big Sci. **2** (2018) 9, [arXiv:1810.00019](#).
- [44] Belle II Analysis Software Group, J.-F. Krohn *et al.*, Global decay chain vertex fitting at Belle II, Nucl. Instrum. Meth. **A976** (2020) 164269, [arXiv:1901.11198](#).
- [45] Particle Data Group, S. Navas *et al.*, Review of particle physics, Phys. Rev. D **110** (2024) 030001.
- [46] H. Voss, A. Höcker, J. Stelzer, and F. Tegenfeldt, TMVA, the toolkit for multivariate data analysis with ROOT, PoS **ACAT** (2007) 040.
- [47] A. Hoecker *et al.*, TMVA – Toolkit for Multivariate Data Analysis, [arXiv:physics/0703039](#).
- [48] N. L. Johnson, Systems of frequency curves generated by methods of translation, Biometrika **36** (1949) 149.
- [49] F. A. Berends, K. J. F. Gaemers, and R. Gastmans,  $\alpha^3$  contribution to the angular asymmetry in  $e^+e^- \rightarrow \mu^+\mu^-$ , Nucl. Phys. B **63** (1973) 381.
- [50] R. W. Brown, K. O. Mikaelian, V. K. Cung, and E. A. Paschos, Electromagnetic background in the search for neutral weak currents via  $e^+e^- \rightarrow \mu^+\mu^-$ , Phys. Lett. B **43** (1973) 403.
- [51] R. J. Cashmore, C. M. Hawkes, B. W. Lynn, and R. G. Stuart, The forward-backward asymmetry in  $e^+e^- \rightarrow \mu^+\mu^-$  comparisons between the theoretical calculations at the one loop level in the Standard Model and with the experimental measurements, Z. Phys. C **30** (1986) 125.
- [52] A. Valassi, Combining correlated measurements of several different physical quantities, Nucl. Instrum. Meth. A **500** (2003) 391.